PNAS RESEARCH ARTICLE | ENGINEERING
DEVELOPMENTAL BIOLOGY

Mimicking angiogenic microenvironment of alveolar soft-part sarcoma in a microfluidic coculture vasculature chip

Surachada Chuaychob[a], Ruyin Lyu[a], Miwa Tanaka[b,c], Ayumi Haginiwa[a], Atsuya Kitada[a], Takuro Nakamura[c], and Ryuji Yokokawa[a,1]

Edited by Napoleone Ferrara, University of California San Diego, La Jolla, CA; received July 27, 2023; accepted January 24, 2024

Alveolar soft-part sarcoma (ASPS) is a slow-growing soft tissue sarcoma with high mortality rates that affects adolescents and young adults. ASPS resists conventional chemotherapy; thus, decades of research have elucidated pathogenic mechanisms driving the disease, particularly its angiogenic capacities. Integrated blood vessels that are rich in pericytes (PCs) and metastatic potential are distinctive of ASPS. To mimic ASPS angiogenic microenvironment, a microfluidic coculture vasculature chip has been developed as a three-dimensional (3D) spheroid composed of mouse ASPS, a layer of PCs, and endothelial cells (ECs). This ASPS-on-a-chip provided functional and morphological similarity as the in vivo mouse model to elucidate the cellular crosstalk within the tumor vasculature before metastasis. We successfully reproduce ASPS spheroid and leaky vessels representing the unique tumor vasculature to assess effective drug delivery into the core of a solid tumor. Furthermore, this ASPS angiogenesis model enabled us to investigate the role of proteins in the intracellular trafficking of bioactive signals from ASPS to PCs and ECs during angiogenesis, including Rab27a and Sytl2. The results can help to develop drugs targeting the crosstalk between ASPS and the adjacent cells in the tumoral microenvironment.

angiogenesis | microenvironment | alveolar soft-part sarcoma | spheroid | trafficking

Significance

The in vitro model of alveolar soft-part sarcoma (ASPS) comprehensively mimicked the complex angiogenesis ASPS environment with abundant pericytes-rich and perfusable vascular networks. Compared to the conventional avascular tumor spheroid models, our ASPS-on-a-chip, comprising a mouse ASPS spheroid and pericyte-endothelial cell coculture, replicates the in vivo tumor vasculature that is rich in pericytes, enabling the study of cellular interactions before metastasis. Besides, the ASPS-on-a-chip provided functional and morphological similarity as the in vivo mouse model, which helps to investigate the role of Rab27a and Sytl2 in intracellular signaling during tumor vessel formation. These findings are crucial for developing targeted therapies that disrupt the cellular communication within the tumor microenvironment, potentially offering broad avenues for ASPS treatment.

Tumor-on-a-chip (ToC) is a promising approach to develop tumor models (1, 2) that simplify the self-organization of cells in static cell cultures (3) and the pathophysiological tumor microenvironment (4). ToCs have been explored over the last decade because these chips recapitulate human physiology more accurately than animal models (5–7). The integration of cell culture and microfluidic technology enables the design of a specific tumoral microenvironment suitable for elucidating cell responses to the environment (8), the evaluation of drug efficacy in drug screening (9–11), and the test of therapeutic applications (12) prior to human clinical trials.

Furthermore, the combination of a three-dimensional (3D) tissue culture (a tumor spheroid) with a microfluidic coculture vasculature chip can recapitulate specific cellular pathways, human tissue microenvironments, and it can potentially assemble as a 3D solid tumor (3, 8, 13) and capillary blood vessels (8, 13). Even if transgenic mice are the most common models to recapitulate tumors of immunocompromised patients with specific gene mutations (14–18), animal models involve ethical problems (19–21) that do not exist with in vitro preclinical platforms. Most importantly, elucidating molecular mechanisms such as cell–cell and cell–microenvironment interactions is not possible using animal models.

Herein, we developed a microfluidic coculture vasculature chip and focused on replicating a rare solid tumor, namely alveolar soft-part sarcoma (ASPS) (22–25), and its ability to recruit blood vessels through angiogenesis. Integrated blood vessels rich in pericytes and metastatic capacity are essential characteristics of ASPS suitable to be analyzed with a ToC approach. In addition, ASPS resists conventional chemotherapy (26), and thus, decades of research have elucidated pathogenic mechanisms driving the disease, particularly its angiogenic behavior. By using the proposed ToC preclinical model, tissue-level physiological interactions and manifestations of the disease are more similar to in vivo conditions of ASPS than in animal models, improving our understanding of ASPS pathophysiology. Such results could help in ASPS drug development, and the coculture vasculature chip could be a ready-to-use platform for preclinical drug screening of ASPS treatments.

Hence, the ASPS angiogenic microenvironment was mimicked using a mouse ASPS spheroid in a microfluidic coculture vasculature chip. Pericytes (PCs) in the layer of endothelial cells (ECs) positively influenced the formation of a mouse ASPS spheroid, recruiting tumor vasculature through the platelet-derived growth factor β (Pdgfb) signaling pathway (27) since PCs contribute to angiogenic initiation and vessel stability in both tumor and non-tumor cells. In addition, the present study confirmed that Pdgfb and

Author contributions: S.C., M.T., T.N., and R.Y. designed research; S.C., R.L., M.T., A.H., and A.K. performed research; T.N. and R.Y. contributed new reagents/analytic tools; S.C., R.L., M.T., T.N., and R.Y. analyzed data; and S.C., M.T., T.N., and R.Y. wrote the paper.

The authors declare no competing interest.

This article is a PNAS Direct Submission.

[1]To whom correspondence may be addressed. Email: yokokawa.ryuji.8c@kyoto-u.ac.jp.

This article contains supporting information online at https://www.pnas.org/lookup/suppl/doi:10.1073/pnas.2312472121/-/DCSupplemental.

Published March 19, 2024.

glycoprotein non-metastatic melanoma protein B (Gpnmb) (28) pathways increased ASPS angiogenesis with the participation of Rab27a and Sytl2 that facilitate intracellular transport of cytoplasmic vesicles (25, 29, 30). Rab27a and Sytl2 are direct transcriptional targets of ASPSCR1-TFE3, which is overexpressed in ASPS (25). The ASPS-on-a-chip provides the vascularized and perfusable ASPS spheroid within a microfluidic chip which is different from a widely-used avascular tumor models. The distinctive blood vessel characteristics that are rich in PCs are well constructed by coculturing PCs, and ECs in a microfluidic chip where the perfusable vascular networks are connected to the core of the spheroid. The microfluidic coculture vasculature chip faithfully resembles the vascularized ASPS solid tumor with abundant PCs-rich tumor networks, being a robust drug screening platform for ASPS and contributing to developing drugs that target the cellular crosstalk during the ASPS angiogenesis process.

Results

Feasibility of ASPS Angiogenesis Modeling in a Microfluidic Chip. To investigate the on-chip microenvironment of ASPS angiogenesis, a 3D spheroid of mouse ASPS cells was used to represent a natural solid tumor (*SI Appendix*, Fig. S1 *A* and *B*). This experiment used two types of mouse ASPS cells as an ASPS tumor sample and its negative control (Fig. 1*A*). AS17 cells, the tumoral cells of interest, are mouse ASPS cells expressing the ASPSCR1-TFE3 fusion gene created in an ex vivo mouse model (25, 31). Meanwhile, Null cells, the negative control, are AS17 cells that lose the expression of the ASPSCR1-TFE3 fusion gene (25). As a result, Null cells were lost in vivo tumorigenic activity due to defects in angiogenesis.

The average diameter of AS17 and Null spheroids was 519.3 ± 8.7 and 503.5 ± 13.5 μm, respectively (*SI Appendix*, Fig. S1 *C* and *D*), which could be injected into the microfluidic channel with 100-μm height through a 1-mm injection inlet (*SI Appendix*, Fig. S1*A*). The fluorescence of DsRed-AS17 and DsRed-Null cells could be observed under a fluorescent microscope (Fig. 1*B*). After the on-chip spheroids were incubated overnight in a 37 °C CO_2 incubator, the migration of ASPS cells was observed as the spheroid was actively growing and migrating in this microenvironment. It implies that this injection process does not affect the cell proliferation due to a flexible structure of the spheroid. Then, the layer of GFP-human umbilical vein endothelial cells (GFP-HUVECs) was constructed (Fig. 1*A* and *SI Appendix*, Fig. S1 *A* and *B*). Accordingly, the angiogenesis study started at this point, defined as day 0 (*SI Appendix*, Fig. S1*B*).

Angiogenic sprouts were tracked over 11 d by capturing their green fluorescent signal (top view of the device, Fig. 1*B*) to analyze the sprout coverage area (Fig. 1*C*), invasion area of sprout penetrating the core of spheroid (Fig. 1*D*), and migration area of ASPS cells from the core of spheroid (Fig. 1*E*). The culture medium was changed daily to maintain a static cell culture. During on-chip coculture of the spheroid, the growth of angiogenic sprouts toward the spheroid was observed (Fig. 1*B*). In particular, the top view images on day 11 showed many sprouts that penetrated the spheroid (Fig. 1*B*). Furthermore, a significant difference in sprout coverage area was observed from day 7 compared to the negative control (Fig. 1*C*), while there was no significant difference in the invasion area between AS17 and Null cells (Fig. 1*D*). Interestingly, AS17 and Null cells were growing well in the device, resulting in a gradual spheroid migration covering the whole area in the middle channel (Fig. 1*E*) and migration to the side channels (*SI Appendix*, Fig. S1*E*). These findings enabled us to evaluate the dynamic of ASPS angiogenesis on the induction of angiogenic sprouts cultured over several days (Fig. 1*F*). Many angiogenic sprouts invaded the spheroid in x, y, and z directions, evidently observed at the bottom, middle, and top planes (Fig. 1*F* and *SI Appendix*, Fig. S1*F*), as well as on a z-projection image.

Optimum Ratio of PCs to ECs for the Recruitment of Tumor Vasculature. To mimic natural blood capillaries, PCs usually wrap around ECs that line the capillaries and venules throughout the body (32). They regulate blood flow and maintain homeostasis (33). In addition, PCs are essential in tumor angiogenesis as they promote EC survival and migration, which aids tumor vascularization (34) (*SI Appendix*, Fig. S2*A*). The proper ratio of ECs to PCs is the first criterion to recapitulate tumor angiogenesis in vitro. It was expected that a high concentration of PCs would create a better coculture vascular network, allowing for the preservation of the mature vascular network in a chip for future studies. Thus, non-labeled PCs and GFP-HUVECs were cocultured with DsRed-ASPS spheroids (Fig. 2 *A* and *B* and *SI Appendix*, Fig. S2*B*), and ECs:PCs ratios of 80:1, 20:1, and 5:1 were studied (Fig. 2 *B*–*G*). The ratio that provided a vascularized tumor spheroid was chosen as the optimum coculture condition. Within 3 culturing days, the percentage of sprout coverage area in Fig. 2*C* and invasion area in Fig. 2*D* showed that a high concentration of PCs induced more angiogenic sprouts and vascular invasion into the spheroid core than a low concentration of PCs. As expected, PCs induce more angiogenic sprouts in the coculture (ECs:PCs) microenvironment (Fig. 2*B*) compared to the monoculture (EC-alone) microenvironment (Fig. 1*B*, AS17). Remarkably, all ratios induced well-connected vessels with no significant difference in the sprout coverage area from day 7 (Fig. 2*C*). Hence, either one can form vascular networks in a coculture chip. The suitable ratio depends on the purpose of use. The 5:1 ratio is preferable for forming vascular networks where cell–cell crosstalk can be studied, and cells can be localized clearly by immunofluorescent images (Fig. 3). Meanwhile, the 20:1 ratio is promising to replicate an in vivo environment of a vascularized solid tumor where vasculature can be studied further (Fig. 4).

Ability to Elucidate Cell-to-Cell Crosstalk. To clarify the angiogenic mechanism of ASPS, particularly cell–cell crosstalk among ASPS, PCs, and ECs cells, we validate their colocalization in a chip by immunostaining on day 11 (Fig. 3*A*). In the coculture chip using the 5:1 ratio of ECs:PCs, it was expected to find aligned cells, particularly the colocalized ASPS cells-wrapping PCs and colocalized PCs-wrapping ECs (Fig. 3*B*). The bottom plane confocal image clearly showed that PCs colocalized with the vessel network (green) (Fig. 3 *C* and *D*). Furthermore, the migration of ASPS cells toward PCs was evident in the middle plane of the device (Fig. 3 *E* and *F*). In particular, the cell attachment of ASPS and PCs, as well as the migration of PCs toward ECs, were observed in the coculture vasculature chip as shown in the amplified orthogonal views of y-z (Fig. 3*H*) and x-z planes (Fig. 3*I*) of the top plane of the device (Fig. 3*G*), where the core spheroid was located.

Characterization of the Vascularized ASPS Spheroid and Tumor Vasculature. The ratio of ECs:PCs at 20:1 was utilized to coculture AS17 and Null spheroids to study ASPS angiogenic recruitment (Fig. 4*A*). The sprout coverage and invasion areas, as well as spheroid migration, are relevant parameters that indicate the resemblance of ASPS angiogenesis in vitro. Clearly, AS17 spheroids significantly recruited more angiogenic sprouts than the Null spheroids (Fig. 4*B*), with a significant difference in the sprout coverage area after 3 d of culture (Fig. 4*C*). In addition,

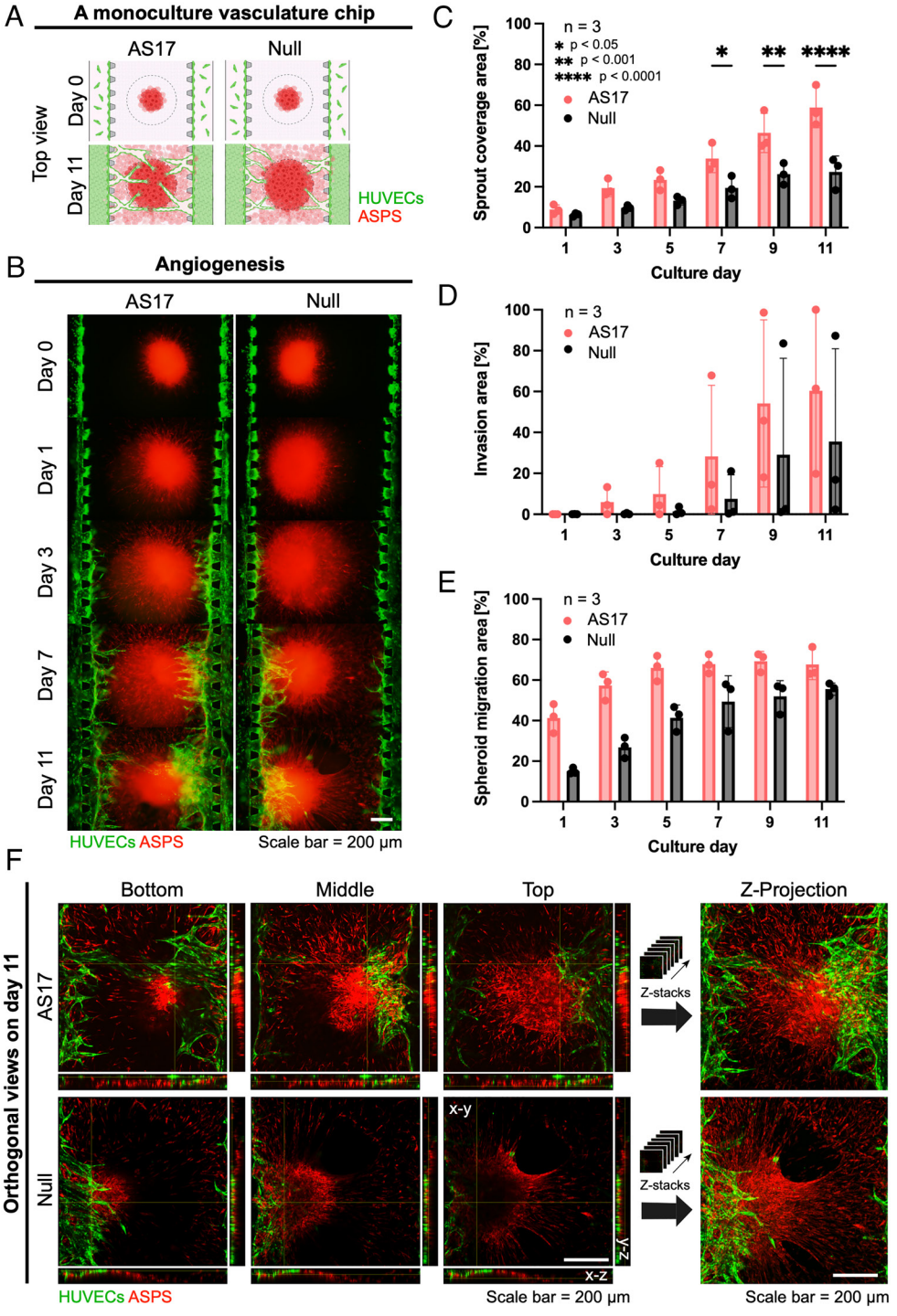

Fig. 1. Mimicking angiogenic microenvironment of ASPS in a monoculture vasculature chip. (*A*) Illustration of ASPS angiogenesis in a monoculture (EC alone) vasculature chip. (*B*) Fluorescence overlay images of angiogenic sprouts (GFP-HUVECs, green) induced by DsRed-AS17 and DsRed-Null spheroids (red) during 11 culture days. The fluorescence images were captured with a ×10 magnification from the top view of the microfluidic device focusing on the middle channel. (*C*) Percentage of sprout coverage area over time. (*D*) Percentage of invasion area over time. (*E*) Percentage of spheroid migration area over time. Data are presented as average values ± SD, n = 3. Statistical analysis was performed using two-way ANOVA. (*F*) Orthogonal views and their z-projection of confocal images of AS17 and Null spheroids with angiogenic sprouts on day 11 at the bottom, middle, and top planes of the microfluidic device. GFP-labeled HUVECs and DsRed-labeled ASPS are in green and red, respectively.

the percentage of the sprouts that invaded the spheroids' core differed significantly between the AS17 and Null spheroids after 5 d of culture, reaching 100 % invasion from the 7th day of culture (Fig. 4*D*). These results highlight the synergy between PCs and ECs on ASPS angiogenesis to form the vascularized spheroid and the connected vascular networks rich in PCs. Furthermore, the coculture system provided a friendly environment for the spheroid culture on a chip, considering the gradual increase of migration of AS17 and Null spheroids in the middle channel of the microfluidic device (Fig. 4*E*).

The enhancement of tumor vessel perfusability and permeability toward the coculture ECs:PCs with an AS17 spheroid were studied (Fig. 4*F*) to characterize the vessel perfusability and the tumor vasculature phenotype (34). The coculture ECs:PCs with a human lung fibroblast (hLF) spheroid was utilized as a negative control (Fig. 4*G*). hLF cells represent non-tumor cells that induce normal vasculatures (35). The tumor and non-tumor vessels were then verified by injecting a fluorescent dye solution (BSA-Alexa Flour 647). The dynamic time-lapsed images at 0, 5, 10, 15, 30, 200, 400, and 600 s were utilized for comparison. The coculture ECs:PCs (20:1) with an AS17 spheroid clearly showed the perfusable vessels with high permeability (Fig. 4*H*) where the solution of interest, BSA-Alexa Fluor 647 (magenta), flowed through from the right-handed side of the device into the center of the spheroid within 5 s (Fig. 4*H*, t = 5 s), and reached the left-handed side of the device in 30 s (Fig. 4*H*, t = 30 s). The coverage area of

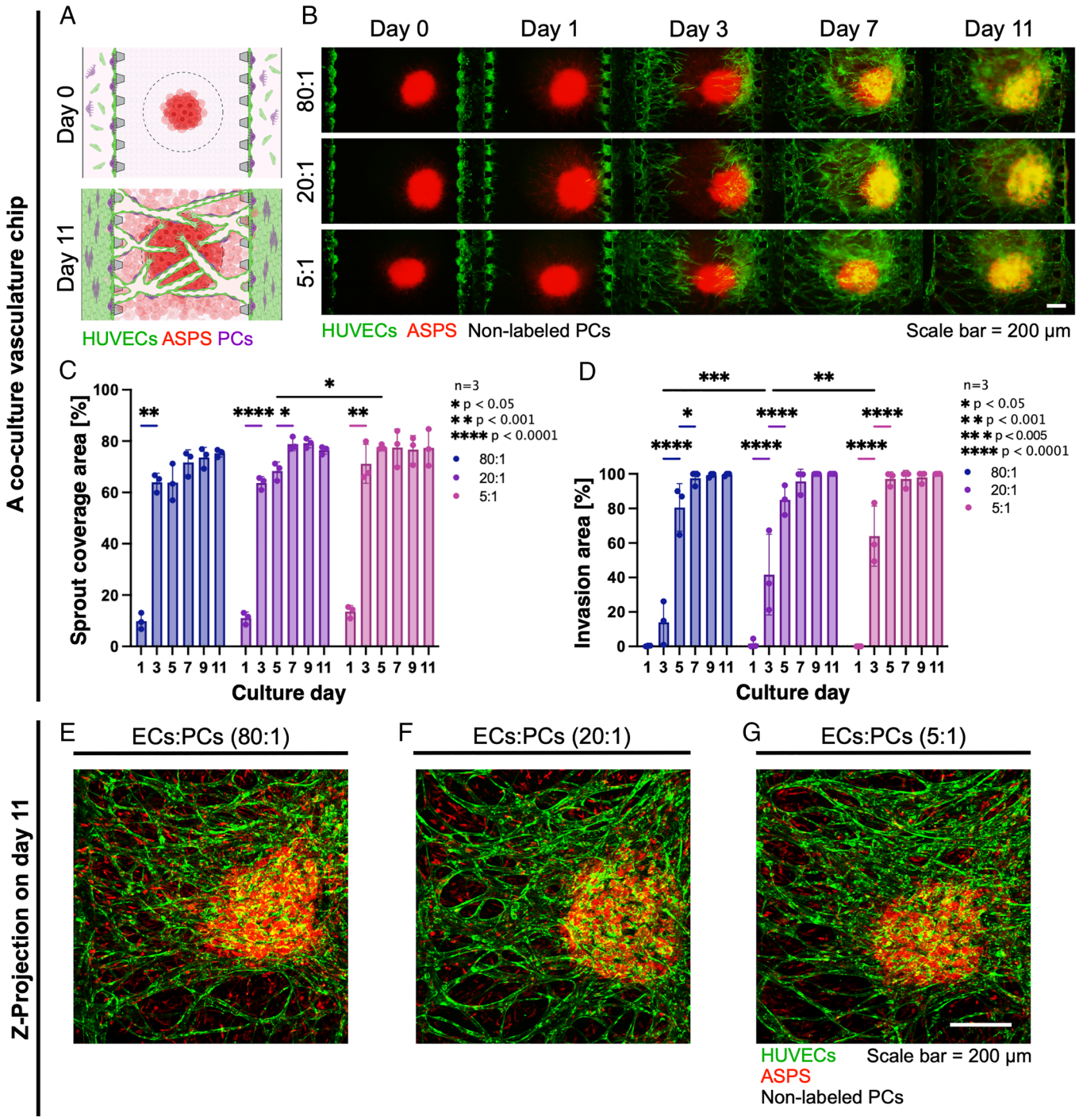

Fig. 2. Mimicking angiogenic microenvironment of ASPS in a coculture vasculature chip. (*A*) Illustration of the coculture vasculature device (top view) on days 0 and 11. (*B*) Fluorescence overlay images of angiogenic sprouts (GFP-HUVECs, green) induced by DsRed-AS17 spheroids (red) with different with ECs:PCs ratios of 80:1, 20:1, and 5:1 during 11 culture days. The fluorescence images were captured with a ×10 magnification from the top view of the microfluidic device focusing on the middle channel. (*C*) Percentage of sprout coverage area over time. (*D*) Percentage of invasion area over time. Data are presented as average values ± SD, n = 3. Statistical analysis was performed using two-way ANOVA. (*E*–*G*) Fluorescence overlay images of angiogenic sprouts and their confocal images (z-projection) on day 11 on the recruitment of tumor vasculature with ECs:PCs ratios of 80:1, 20:1, and 5:1. The fluorescence and confocal images were captured with a ×10 magnification from the top view of the microfluidic device focusing at one middle channel. In (*E*–*G*), GFP-labeled HUVECs and DsRed-labeled ASPS are in green and red, respectively, while PC is colorless.

fluorescent solution inside (In) and outside (Out) of the core spheroid was determined over time (Fig. 4*I*). As expected, the coverage area inside the core spheroid reached 100 % and remained constant within 30 s, showing that the solution of interest completely diffused from the vasculatures into the vascularized spheroid (Fig. 4*I*, In). The vasculatures outside the spheroid could deliver the solution without leaking, as clearly seen at 5, 10, and 15 s. Eventually, the dye solution leaked and gradually covered the whole area outside the core of the spheroid (Fig. 4*I*, Out), showing a characteristic tumor vasculature (*SI Appendix*, Fig. S3). On the contrary, the non-tumor spheroid recruiting the normal vessel showed lower vessel permeability in the same period than that of a tumor spheroid (Fig. 4*J*). The dye flowed through and remained in the vessel for 200 s (Fig. 4*J*, t = 200 s) before it was slowly permeabilized,

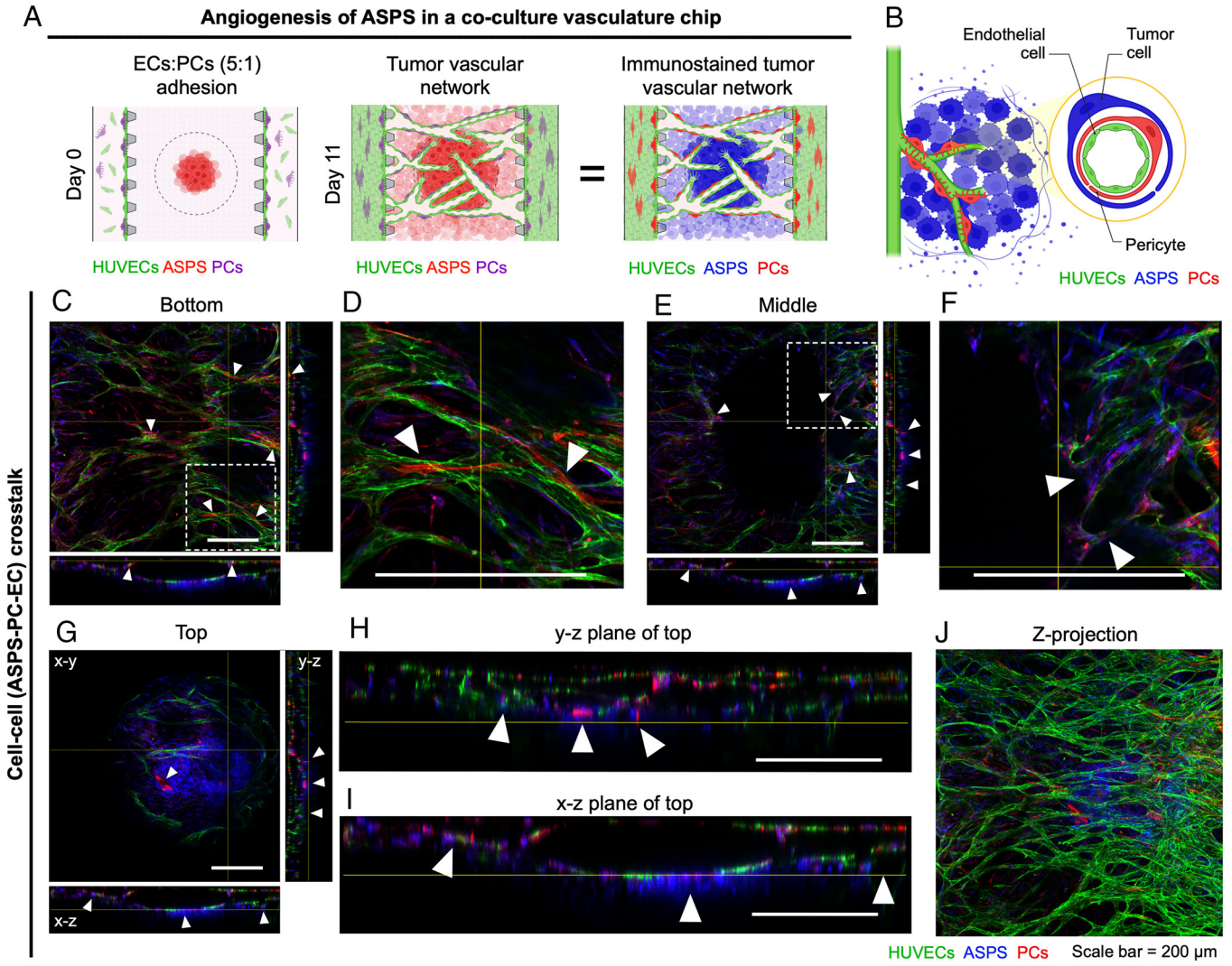

Fig. 3. Angiogenic microenvironment of ASPS in a coculture (5:1) vasculature chip. (*A*) Illustration of the coculture (5:1) vasculature device before and after immunohistochemical treatment on day 11. (*B*) Illustration of ASPS-wrapped PC and EC in the ASPS tumor microenvironment. (*C*) Orthogonal views at the bottom plane and (*D*) their magnification of confocal images of an AS17 spheroid with coculture ECs:PCs (5:1) on day 11 in the microfluidic device (white dashed box). White arrowheads indicate the attachment of cells to pericytes surrounding the tumor vessel. (*E*) Orthogonal views at the middle plane and (*F*) their magnification of confocal images in the same device. White arrowheads indicate the localization of ASPS cells that surround the pericytes. (*G*) Orthogonal views at the top plane and their magnification of (*H*) y-z, and (*I*) x-z planes in the same device. White arrowheads indicate cell–cell crosstalk of ASPS surrounding the pericytes that wrap the tumor vessel. (*J*) Z-projection image of the device. The 3D vasculature with pericytes penetrates the spheroid core. In (*C–J*), anti-Flag detects Flag-tagged ASPSCR1-TFE3 in ASPS cells (blue), anti-CD31 detects CD31-mediated endothelial cell-to-cell interaction (green), and anti-alpha-smooth muscle actin detects microfilament bundles of pericytes (red).

representing a normal vasculature (*SI Appendix*, Fig. S3). Hence, the coverage area of dye In and Out significantly differed between tumor (Fig. 4*I*) and non-tumor vessels (Fig. 4*K*).

Indirect Evaluation of Signaling Protein Delivery in Angiogenic Sprout Recruitment. To deliver signaling proteins, such as Gpnmb (25, 27) and Pdgfb (25, 28), outside the ASPS cells to recruit angiogenic sprouts from the vessels rich in PCs, intracellular trafficking proteins, particularly Sytl2 and Rab27a (25, 29, 30), are essential vehicles during angiogenesis. Hence, sgSytl2 cells and sgRab27a cells, the knockout (KO) Sytl2 and Rab27a with a target control single guide (sg) RNA in AS17 cells, were compared with sgNTC AS17 cells, which are AS17 cells with a non-target control sgRNA, as a positive control. The same experiment was performed using the Null cells as a negative control. The diameter of sgNTC, sgRab27a, and sgSytl2 spheroids built with 1.25×10^5 cells mL^{-1} was 825.9 ± 24.5, 453.8 ± 12.2, and 847.7 ± 24.3 μm, respectively (*SI Appendix*, Fig. S1*D*). First, the ability to recruit angiogenic sprouts was compared among different ASPS cells under the same condition. It was found the sgNTC spheroid induced the most abundant angiogenic sprouts over 11 d of culture, while Null, sgSytl2, and sgRab27a spheroids recruited significantly fewer amount of angiogenic sprouts than those of the sgNTC spheroid, as shown in the fluorescence images (Fig. 5*A*) and the confocal z-stack and orthogonal-view images (Fig. 5*B*). Consistently, angiogenic sprouts were induced to 90 % coverage area on day 11 by the sgNTC spheroid, whereas other spheroids induced sprouts at a coverage area of less than 40, 50, and 60 % for the sgRab27a, sgSytl2, and Null spheroids, respectively (Fig. 5*C*). The significant reduction in angiogenic sprout recruitment by the KO Rab27a and Sytl2 ASPS cells proves their critical role in the intracellular transport of cytoplasmic vesicles to deliver signaling proteins in ASPS angiogenesis (Fig. 5*D*).

Direct Evaluation of Signaling Protein Delivery Inside the ASPS Cell During Angiogenic Sprout Recruitment. Three tumor microenvironments were analyzed; 1) an AS17 spheroid without

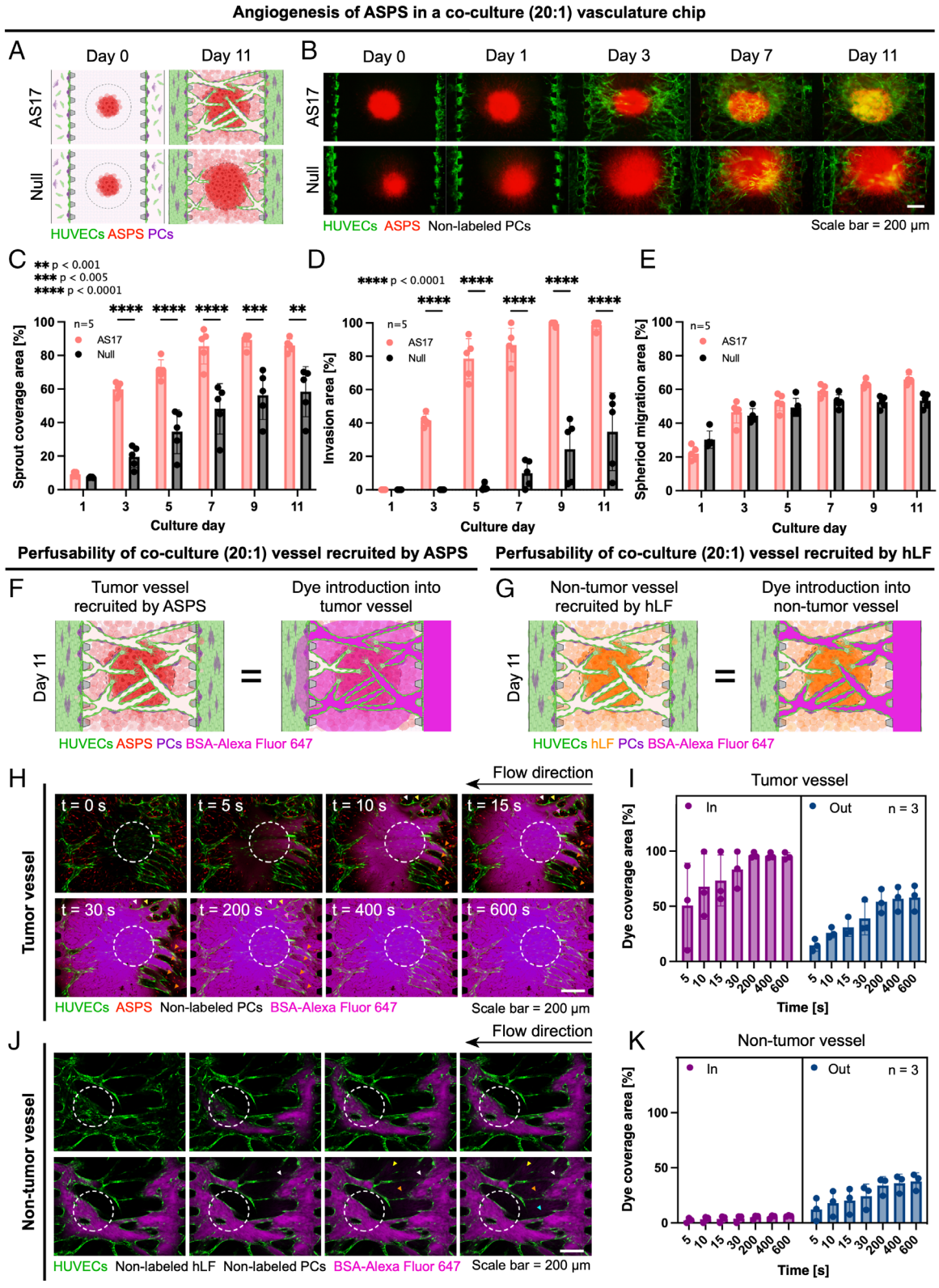

Fig. 4. Characteristics of tumor vasculatures and a vascularized ASPS spheroid in the coculture vasculature chip. (*A*) Illustration of the coculture (20:1) vasculature device. (*B*) The fluorescence overlay images of an AS17 spheroid with ECs:PCs (20:1) vascular networks during 11 culture days. The fluorescence images were captured with a ×10 magnification from the top view of the microfluidic device focusing on the middle channel. (*C*) Percentage of sprout coverage area over time. (*D*) Percentage of invasion area over time. (*E*) Percentage of spheroid migration area over time. The data are presented as average values ± SD, n = 5. Statistical analysis was performed using two-way ANOVA. (*F*) Illustration of perfusability evaluation of coculture (20:1) vessels recruited by ASPS. (*G*) Illustration of perfusability evaluation of coculture (20:1) vessels recruited by hLF. (*H*) Time-lapsed images of an AS17 spheroid-induced tumor vessel on day 11. The fluorescent dye BSA-Alexa Fluor 647 is injected from channel 3 to study the perfusability and permeability of the vessels. The flow direction is from right to left. GFP-labeled HUVECs and DsRed-labeled ASPS are in green and red, respectively, while PC is colorless. BSA-Alexa Fluor 647 is magenta. The dashed circle indicates the location of a spheroid core. Color arrowheads indicate the starting point of dye leakage from the vessel. (*I*) Percentage of dye coverage area at different time points inside and outside a spheroid core from a tumor vessel. Data are presented as average values ± SD, n = 3. (*J*) Time-lapsed images of a hLF spheroid-induced non-tumor vessel on day 11. Color arrowheads indicate the starting point of dye leakage from the vessel. (*K*) Percentage of dye coverage area at different time points inside and outside a spheroid core from a non-tumor vessel. The data are presented as average values ± SD, n = 3. In (*B*, *H*, and *J*), GFP-labeled HUVECs are green, while hLF and PC are colorless. BSA-Alexa Fluor 647 is magenta.

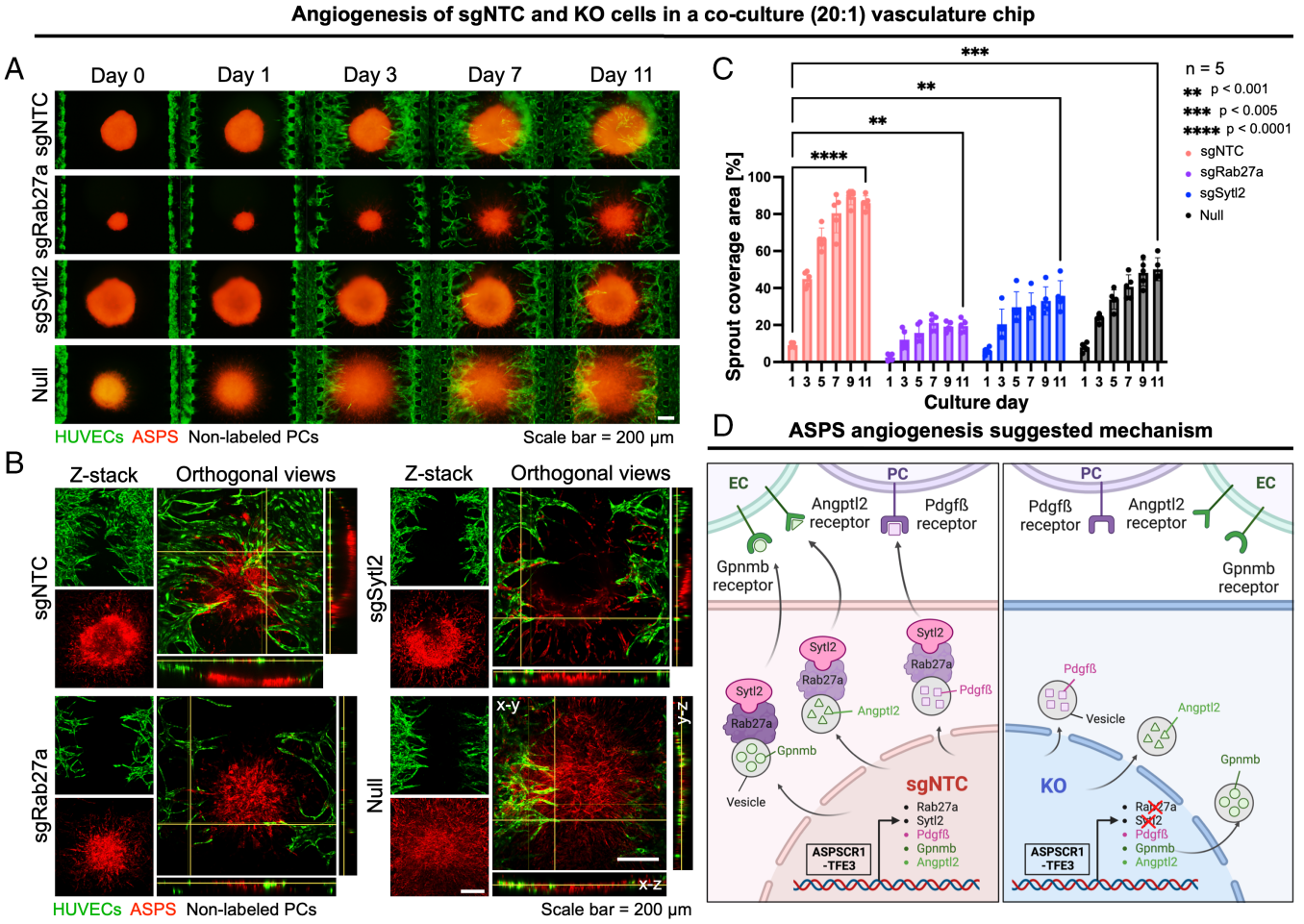

Fig. 5. Role of intracellular trafficking proteins in ASPS angiogenesis recruitment using KO cells. (*A*) The fluorescence overlay images of KO spheroids (sgRab27a and sgSytl2) and their positive and negative control spheroids (sgNTC and Null) with ECs:PCs (20:1) vascular networks during 11 culture days. The fluorescence images were captured with a ×10 magnification from the top view of the microfluidic device focusing on the middle channel. (*B*) Z-stack and orthogonal views of the confocal images of each spheroid with angiogenic sprouts on day 11 in the microfluidic device. GFP-labeled HUVECs and DsRed-labeled ASPS are in green and red, respectively, while PC is colorless. (*C*) Comparison of the percentage of sprout coverage area over time. Data are presented as average values ± SD, n = 5. Statistical analysis was performed using two-way ANOVA. (*D*) Illustration of ASPS angiogenic suggested mechanism. Signaling proteins (Gpnmb, Angptl2, and Pdgfb) are delivered with the aid of intracellular trafficking proteins (Rab27a and Sytl2) from an ASPS cell, such as an sgNTC cell, to an EC and PC cell during ASPS angiogenic progression.

vasculature on day −1; 2) an AS17 spheroid with monoculture (EC alone) vasculature on day 11; and 3) an AS17 spheroid with coculture (ECs:PCs at 20:1) vasculature on day 11, representing the natural blood capillaries (Fig. 6). In Fig. 6 *A*–*F*, immunofluorescence images showed DAPI (yellow) and anti-flag® M2 antibody (blue) detecting nuclei and Flag-tagged ASPSCR1-TFE3, respectively. Pdgfb protein (red) was positive to anti-PDGF B antibody. Gpnmb protein (red) was positive to mouse oseteoactivin/GPNMB antibody. The spheroid without vasculature showed less expression of Pdgfb and Gpnmb (Fig. 6 *A* and *D*) compared to the AS17 spheroid with monoculture vasculature (Fig. 6 *B* and *E*). Interestingly, the highest accumulation of Pdgfb and Gpnmb was observed in the coculture vasculature condition with the AS17 spheroid (Fig. 6 *C* and *F* and *SI Appendix*, Fig. S4), owing to the synergistic cell–cell communication of ECs:PCs and ASPS cells. The Null spheroid system, however, did not show significant expression of Pdgfb and Gpnmb in the tumor microenvironments (*SI Appendix*, Fig. S5). Most importantly, Pdgfb and Gpnmb expression from the in vitro coculture vascularized ASPS spheroid correlate well with those from in vivo mouse models (Fig. 6*G*). Histologic analysis showed that the tumors expressing ASPSCR1-TFE3 were surrounded by pericytes (arrowhead) (31). The nuclei were positive for Flag-tagged ASPSCR1-TFE3, while the accumulation of Pdgfb and Gpnmb was positive to anti-PDGF B and Mouse oseteoactivin/GPNMB antibodies, respectively.

Discussion

This study aimed to develop a model that recapitulates the angiogenic microenvironment of ASPS before its metastatic stage. The monoculture vasculature of the ASPS microenvironment confirmed the feasibility of ASPS-on-a-chip. It was found that angiogenic sprouts could be induced by the 3D spheroid constructed solely from ASPS tumor cells (Fig. 1*A*), clearly observed as an increase in the sprout coverage area (Fig. 1*C*). This ensured we successfully cultured an ASPS spheroid, representing a solid tumor, which recruits angiogenic sprouts differently from a Null spheroid under the simplified microenvironment of a microfluidic chip.

Furthermore, the functional and morphological similarity as the in vivo mouse model (25, 31) of ASPS is recapitulated on a microfluidic chip using the coculture vasculature between PCs and ECs, thereby enhancing the growth of angiogenic sprouts induced by ASPS tumor cells (Fig. 2). The cell–cell crosstalk can be elucidated in the coculture vasculature device, and cell localization can be observed at the microfluidic scale via the migration of ASPS cells toward PCs (Fig. 3 *C*–*J*), considering that ASPS secretes Pdgfb

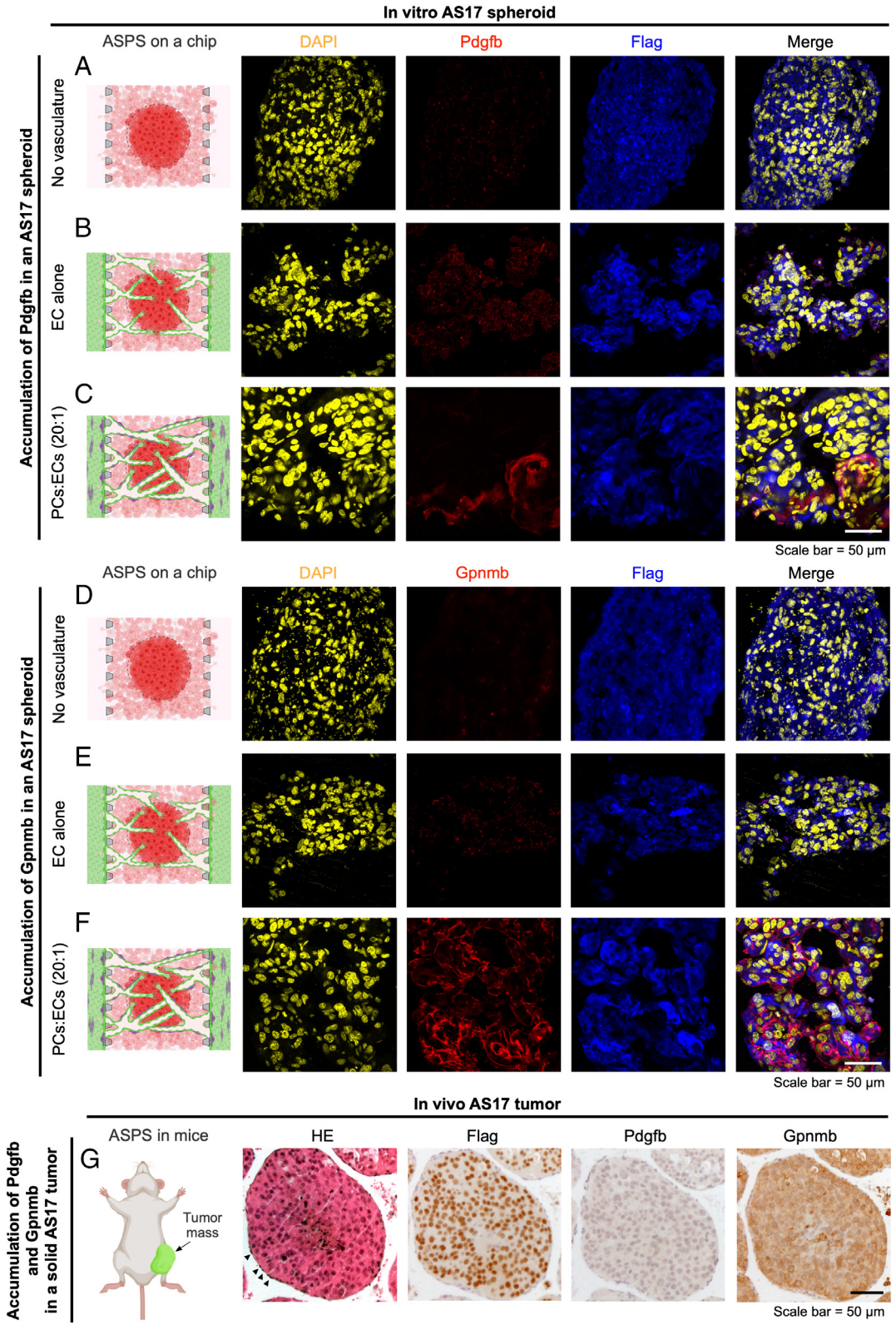

Fig. 6. Signaling proteins delivered with the aid of intracellular trafficking proteins in the coculture (20:1) vasculature chip. Representative fluorescence images of an in vitro AS17 spheroid with accumulation of Pdgfb in different tumor microenvironments; (*A*) no vasculature, (*B*) monoculture vasculature (EC alone), and (*C*) coculture ECs:PCs (20:1). The ASPS cells were determined by immunofluorescence staining with DAPI detecting nuclei (yellow), anti-PDGF B antibody detecting Pdgfb (red), and Anti-flag® M2 antibody detecting Flag-tagged ASPSCR-TFE3 (blue). Representative fluorescence images of an in vitro AS17 spheroid with the accumulation of Gpnmb in different tumor microenvironments; (*D*) no vasculature, (*E*) monoculture vasculature (EC alone), and (*F*) coculture ECs:PCs (20:1). The ASPS cells were determined by immunofluorescence staining with DAPI detecting nuclei (yellow), mouse oseteoactivin/GPNMB antibody detecting Gpnmb (red), and Anti-flag® M2 antibody detecting Flag-tagged ASPSCR1-TFE3 (blue). (*G*) H&E staining and immunohistochemical analysis of an in vivo ASPS tumor. H&E showed ASPS cells expressing ASPSCR1-TFE3 surrounded by pericytes (arrowhead). Immunostaining images showed the Flag-tagged ASPSCR1-TFE3 marker for ASPS cells and Gpnmb, and Pdgfb markers for accumulation of Gpnmb and Pdgfb proteins in ASPS cells.

that stimulates the proliferation of PDGFRB-expressing pericytes. In addition, these on-chip results are consistent with the mouse model previously reported by Tanaka and Nakamura (25).

Using an ex vivo mouse model (31), angiogenesis was proposed to happen through the migration of ASPS cells toward pericytes to receive cytokines, and through the receptor recruitment on ASPS cell membrane promoted by intracellular trafficking proteins, such as Sytl2 and Rab27a. Then, PCs proliferate toward Pdgfb secreted by ASPS cells, accelerating the formation of a mature vascular network through bioactive signals, such as Angiopoietin-related protein 2 (Angptl2) and Vascular endothelial growth factor (Vegf). However, the inherent complexity of in vivo models impedes proving this mechanism.

Nonetheless, the same phenomena were observed using the microfluidic coculture device, confirming that the crosstalk between ASPS and PCs (Fig. 3 *G–I*), as well as between PCs and ECs (Fig. 3 *C–F*), enhanced the angiogenesis of ASPS (Fig. 3*J*) as proposed by the analysis of the mouse model developed by Tanaka and Nakamura. Our study emphasizes the essential role of the in vitro model in simplifying the tumor microenvironment, allowing us to confirm cell–cell crosstalk and expand the previous in vivo results.

Pericytes-associated endothelial cells were enriched in the mature tumor vasculatures and the vascularized ASPS spheroid. These results mirror in vivo phenotypes where tumor cells harbor active blood capillaries (Fig. 3 *A–F*). We noted a significantly higher sprout coverage and invasion areas of AS17 cells compared to Null cells in coculture conditions, presuming that ASPS cells activate an angiogenic-related signaling mechanism at early stages. The tumor vasculature has higher permeability than that of normal vasculature, with significant leakage in the spheroid core (Fig. 4*H*). This study shows that the tumor vasculature predominates in the coculture vasculature device in proportion to the degree of vascularization of the spheroid core (Fig. 4*I*). This characteristic is an advantage for future drug screening testing since the coculture vasculature delivers the solution of interest into the core of the vascularized tumor spheroid and allows its fast diffusion to tumor cells through the leaky vascular networks. This shows that our system recapitulated the in vivo-like phenomenon of ASPS angiogenesis and allowed us to elucidate cell–cell crosstalk that is technically challenging to study in an animal model (19–21).

The role of intracellular trafficking proteins was successfully elucidated in the microfluidic coculture vasculature chip (Figs. 5 and 6). The induction of tumor vessels by an ASPS spheroid happened with the aid of Rab27a and Sytl2 proteins that carry signaling proteins such as Pdgfb, Gpnmb, and Angptl2, from an ASPS cell to a pericyte and an endothelial cell, confirmed through KO conditions (Fig. 5). The role of proteins in intracellular vesicular transport is confirmed by comparing the conditions without Rab27a (sgRab27a cells) or Sytl2 (sgSytl2 cells) to the positive and negative controls, sgNTC and Null cells, respectively (Fig. 5 *A* and *B*). In Fig. 5*A*, the sgRab27a spheroid shows smaller in size on day 0 comparing with other spheroids due to its innate behavior even if the numbers of seeding cell are the same. However, a microfluidic device can neglect those concerns. A significant decrease in sprout coverage area was observed in sgRab27a or sgSytl2 cells compared to the positive control and less than or equal to the negative control (Fig. 5*C*). We noted the participation of intracellular trafficking proteins in coculture conditions and highlighted that signaling proteins were delivered to adjacent cells, initiating the growth of angiogenic sprouts and leading to mature vessels rich in PCs in the ASPS microenvironment (Fig. 5*D*).

These results emphasized the critical role of Rab27a and Sytl2 in the intracellular trafficking of signaling proteins, such as Pdgfb and Gpnmb, from ASPS to neighbor cells, such as PCs and ECs, in ASPS angiogenesis recruitment. Interestingly, the results from both in vitro coculture vasculature chip (Fig. 6 *C* and *F*) and those from the in vivo mouse model (Fig. 6*G*) are similar and representative of ASPS. Accordingly, we hypothesized that the suppression of intracellular trafficking proteins would decrease ASPS angiogenesis. This pilot study demonstrates that ASPS angiogenesis can be restrained by inhibiting Rab27a and Sytl2, providing valuable insight into drug development for ASPS.

To summarize, the microfluidic coculture vasculature chip successfully mimicked the microenvironment of ASPS angiogenesis and was used to analyze the angiogenic mechanism of ASPS. The critical characteristics of the vascularized mouse ASPS spheroid and tumor vessels were demonstrated, providing insight into better drug delivery systems. Microfluidics allows the control of drug molecule gradients in the solution of the well-connected vascular network. Furthermore, the comprehensive data on the induction of ASPS angiogenic behavior disclosed in this work open a broad avenue for developing effective ASPS-specific drugs targeting intracellular trafficking alongside chemotherapy. Furthermore, this microfluidic coculture vasculature chip could be a promising tumor microenvironment on-a-chip model to verify angiogenic mechanisms from other cancer types. Soon, faster, cost-effective alternative microfluidic devices, with flow regulatory systems and multiple unit arrays enabling assays in parallel for high throughput drug screening applications will be necessary.

Materials and Methods

Preparation of the Microfluidic Device. A SU-8 3050 negative photoresist (MicroChem, Westborough, MA) mold patterned by ultraviolet (UV) photolithography was used to fabricate microfluidic devices with 3 100-μm-thick channels. By casting an uncured polydimethylsiloxane (PDMS; Sylgard 184, Dow Corning Toray, Tokyo, Japan) pre-polymer solution with 10:1 (w/w) of PDMS base to curing agent (Silpot, Dow Corning Toray), the PDMS solution was degassed for 2 h in a vacuum chamber followed by curing at 70 °C for 3 to 4 h before peeling from the mold. The spheroid hole, inlets, and outlets were punched with a biopsy punch for 1, 2, and 6 mm in diameter, respectively. The PDMS slab and glass coverslip (24 × 24 mm^2, Matsunami Glass, Osaka, Japan) were cleaned with an adhesive tape and treated with oxygen plasma (40 s, 50 W, flow rate of 50 sccm; Femto Science, Hwaseong, Korea) for irreversible binding. After curing at 70 °C for 12 h, the microfluidic devices were stored in a 40-mm dish (AS ONE Co., Osaka, Japan) and exposed to UV radiation for 2 h before cell seeding experiments.

Cell Culture. The mouse ASPS cell line ASPS17 was prepared to express Flag-tagged ASPSCR1-TFE3 with DsRed fluorescent protein from the tumors induced in embryonic mesenchymal cells as previously described (31). Rab27a and Sytl2 knockout in ASPS cells are achieved by CRISPR/Cas9-mediated gene editing using lentivirus plasmids containing short guided RNA (sgRNA) specific for each gene (*SI Appendix*, Table S1) and they were confirmed by western blotting and/or RT-PCR (*SI Appendix*, Fig. S6) as previously described (25). ASPS cells were grown in Iscove's Modified Dulbecco's Medium with L-glutamine, Phenol Red, HEPES, and Sodium Pyruvate (IMDM, Fujifilm, Osaka, Japan) supplemented with 10 % Fetal Bovine Serum (FBS, Gibco, Grand Island, NY) and 1 % penicillin-streptomycin (P/S, Gibco). The human umbilical vein endothelial cells expressing the green fluorescent protein (GFP-HUVECs, Angio Proteomie, Boston, MA) were cultured in an endothelial growth medium (EGM-2 BulletKit, Lonza, Walkerville, MD) and the fifth passage was used for experiments. Human placental microvascular pericytes (HPMPCs, Angio Proteomie) were cultured in pericyte growth medium (PGM, super rich formulation, Angio-Proteomie) and the sixth passage was used for experiments. The normal human lung fibroblasts (hLFs, Lonza) were cultured in a fibroblast growth medium 2 (FGM-2 BulletKit, Lonza) and the fourth passage was used for experiments. All cells were maintained in a humidified incubator at 37 °C and 5 % CO_2.

Spheroid Preparation. A cell suspension (200 μL, 1.25 × 10^5 cells mL^{-1}) was formed in the U-shaped bottom of a low-binding 96-well plate (Sumitomo Bakelite Co., Tokyo, Japan) within their culture medium. After 2 d in suspension culture at 37 °C and 5 % CO_2, the spheroids were introduced into a microfluidic device.

Cell Culture in the Microfluidic Device. A spheroid suspended in fibrin-collagen type I gel solution [45.5 μL, 2.5 mg mL^{-1} fibrinogen from bovine plasma (Sigma, St. Louis, MO), 0.15 U mL^{-1} aprotinin from bovine lung (Sigma), and 2.0 mg mL^{-1} collagen I, rat tail (Gibco)] was prepared in Dulbecco's phosphate-buffered saline (D-PBS, Takara Bio, Shiga, Japan). After the addition of thrombin (0.5 μL, 0.5 U mL^{-1}, from bovine plasma, Sigma) to initiate gelation, the spheroid solution was immediately injected into the middle of the microfluidic channel through the top hole (spheroid inlet, diameter = 1 mm) with a proper amount of gel filling along the channel without gel leaking. To accelerate gelation, the device with a spheroid was incubated in a 37 °C CO_2 incubator for 15 min, and EGM2 was filled in the side channels to pre-culture the spheroid in a chip for more than 12 h. Cell migration should be observed if the spheroid is actively growing in the microfluidic device. For monoculture (EC alone) vasculature, the layer of ECs was then constructed by injecting a cell suspension in their culture medium (EGM-2, 5.0×10^6 cells mL^{-1}) into channel 1 and tilting the device at 90° to let the cells adhere on the gel surface for 15 min. The layer of ECs in channel 3 was constructed similarly. For coculture (ECs:PCs) vasculature, the mixed layer of ECs and PCs in different ratios was constructed by injecting a constant EC suspension (5.0×10^6 cells mL^{-1}) with various PC ratios in EGM-2 into channel 1 and proceeding similarly as with the monoculture vasculature. After injecting the spheroid and HUVECs into the device, it was kept at 37 °C and 5 % CO_2 in an incubator. The angiogenesis study started at this point, defined as day 0. Meanwhile, the EGM-2 at the inlets of channels 1 and 3 was replaced every day.

Imaging. Bright-field and fluorescent images were captured using an inverted microscope (IX70) with ×4, ×10, and ×20 lenses and a CCD camera (DP80, Evident, Tokyo, Japan). Images were stored in a 16-bit TIFF format using CellSens software (Evident). A confocal microscope (FV3000, Evident) with ×4, ×10, ×20, and ×60 lenses was also used to obtain fluorescent images. Confocal images were stored in a 16-bit TIFF format using FLUOVIEW software (Evident). Fiji (http://fiji.sc.), an open-access software, was used to merge multiple fluorescent images into one image and construct orthogonal and projection views.

Quantification of Sprout Coverage, Invasion, and Spheroid Migration Areas. The sprout coverage area where new angiogenic sprouts were formed in channel 2 was observed using an IX 70 (Evident) microscope. The fluorescent images (GFP-HUVECs) of culturing were converted into 8-bit images and binarized based on a threshold automatically determined by the default setting in the Fiji software. The binarized images of day 0 were subtracted from the images of days 1, 3, 5, 7, 9, and 11. The remaining area with angiogenic sprouts was calculated using the Fiji software. The invasion area where sprouts penetrated the spheroid core was analyzed using the green fluorescent signal (GFP-HUVECs) inside the red fluorescent images (DsRed-ASPS). The spheroid size on day 0 was calculated from the red fluorescent images to indicate the original core size before cell migration. After 8-bit conversion and binarization of GFP-HUVECs images, the binarized images of day 0 were matched with the spheroid size and subtracted from the images of other days. The remaining area inside the designated spheroid core with angiogenic sprouts was calculated using the Fiji software. The spheroid migration area where sprouts grew from the spheroid core was analyzed from the red fluorescent images (DsRed-ASPS). After setting the core spheroid size on day 0, the binarized images of day 0 were subtracted from the images of other days. The remaining area outside the designated spheroid core with migrating cells was calculated using the Fiji software.

Time-Lapse Imaging and Confocal Microscopy. To confirm the perfusability of a vascular network in the microfluidic device, the fluorescent dye (50 μL, 100 μg mL^{-1}) (bovine serum albumin (BSA)-tagged AlexaFluor 647) was observed under a confocal microscope. The dye continuously flowed through the vascular network and spheroid by injecting the dye in the 6-mm inlet of channel 3 (*SI Appendix*, Fig. S1*A*). The flow from the right- to the left-hand side was tracked over 600 s. The 647-channel images were then converted to 8-bit images and binarized. The binarized images at 0 s were then matched with the spheroid size in the DsRed channel and subtracted from the images of other time-lapses. The remaining area inside and outside the spheroid core with flowing dye was calculated using the Fiji software.

Section Samples. All the cells in the microfluidic device were fixed with 4 % paraformaldehyde (PFA, Alfa Aesar, Ward Hill, MA) and stored for 20 min at room temperature. The spheroid was then punched through a 1-mm top hole with a biopsy punch. The punched spheroid was submerged in a Tissue-Tek cryomold (10 mm ×10 mm × 5 mm, Sakura Finetek, Torrance, CA) containing Tissue-Tek O.C.T. compound (Sakura Finetek) and frozen to prepare an embedded spheroid cryoblock. The block was then cryosectioned at 10 μm thickness using a cryostat (Thermo Fisher Scientific, Kalamazoo, MI). For mouse tissue, glutaraldehyde-fixed tumor tissues were embedded in epoxy resin for ultra-thin sections.

Immunohistochemistry. All the cells in the microfluidic device were fixed with 4 % paraformaldehyde (PFA, Alfa Aesar) and stored for 20 min at room temperature. The samples were subsequently treated with 1 % Triton-X 100 (Sigma) at room temperature. The 1 % Triton-X 100 was changed every 15 min three times to permeabilize the cell membrane. Next, 3 % donkey serum (Sigma) was injected into the device and stored for 1 h at room temperature. Afterward, the desired antibodies conjugated to fluorescent dyes (*SI Appendix*, Table S2), such as human alpha-smooth muscle actin Alexa Fluor® 405-conjugated antibody (20 μg mL^{-1}, R&D Systems, Minneapolis, MN), and Alexa Fluor® 647 anti-human CD-31 antibody (100 μg mL^{-1}, BioLegend, SanDiego, CA) at a 1:200 dilution in D-PBS were added to the sample and stored for 48 h at 4 °C for pericyte and vessel staining, respectively. After rinsing with D-PBS, the sample was imaged using a confocal microscope. For immunostaining cryosection samples, all cells on a sectioned slide were fixed with 4 % PFA and stored for 20 min at room temperature. The samples were subsequently treated with 1 % Triton-X 100 for 10 min at room temperature. Next, the slides were treated with 3 % donkey serum and stored for 1 h at room temperature. The slides were treated with the primary antibody overnight at 4 °C. After rinsing with D-PBS, the secondary antibody was applied for 1 h at room temperature. After rinsing the antibody with D-PBS, an antifade solution (Sigma) was applied to the sample, and the slides were properly covered with a cover slip before imaging using a confocal microscope. Primary antibodies (*SI Appendix*, Table S2) such as anti-PDGF B antibody (polyclonal rabbit IgG) (1 mg mL^{-1}, Abcam, Tokyo, Japan), mouse oseteoactivin/GPNMB antibody (polyclonal goat IgG) (0.2 mg mL^{-1}, R&D Systems), and anti-flag® M2 antibody (monoclonal mouse IgG_1) (3.8 to 4.2 mg mL^{-1}, Sigma) were diluted in D-PBS (1:100). Secondary antibodies (*SI Appendix*, Table S2) such as donkey anti-mouse IgG H&L Cy3® 555 (500 μg, Abcam), donkey anti-rabbit IgG H&L Alexa Fluor® 647, preabsorbed (2 mg mL^{-1}, Abcam), and donkey anti-goat IgG H&L highly cross-adsorbed secondary antibody Alexa Fluor® 647 (2 mg mL^{-1}, Abcam) were diluted in D-PBS (1:500). For immunostaining mouse tissue, formaldehyde-fixed, paraffin-embedded tumor tissues were stained with anti-PDGF B antibody (polyclonal rabbit IgG) detecting Pdgfb, Mouse oseteoactivin/GPNMB antibody (polyclonal goat IgG) detecting Gpnmb, and anti-flag® M2 antibody (monoclonal mouse IgG_1) detecting the ASPSCR1-TFE3 antigen (*SI Appendix*, Table S2).

Histopathology. Using standard techniques for light microscopic analysis, formaldehyde-fixed, paraffin-embedded tumor tissues were stained with hematoxylin and eosin (H&E). An anti-flag® M2 antibody (monoclonal mouse IgG_1) with the Histofine Simple Stain Kit (Nichirei, Tokyo, Japan) was used to detect the ASPSCR1-TFE3 antigen. The primary antibodies used for Gpnmb and Pdgfb markers are described in *SI Appendix*, Table S2.

Statistical Analysis. The average spheroid diameters were calculated from 50 independent spheroids. At least three independent spheroids cultured on-chip from each condition were used to analyze the sprout coverage, invasion, and dye coverage areas, as well as spheroid migration. Figure preparation and statistical analysis were performed using GraphPad Prism (GraphPad Software, Boston, MA).

Data, Materials, and Software Availability. All study data are included in the article and/or supporting information.

ACKNOWLEDGMENTS. This work was supported by AMED P-CREATE program [17cm0106609 (T.N.), JP20cm0106277 (T.N. and R.Y.)], AMED P-PROMOTE program [22ama221206h001 (M.T. and R.Y.)], Research on Development of New Drugs [21ak0101170 (T.N.)], AMED-MPS program [JP22be1004204 and JP17be0304205

(R.Y.)], and "Advanced Research Infrastructure for Materials and Nanotechnology in Japan (ARIM)" of MEXT (JPMX1222KT1172), Japan. We would like to thank Editage (www.editage.com) for English language editing. All illustrations created with BioRender.com.

Author affiliations: [a]Department of Micro Engineering, Graduate School of Engineering, Kyoto University, Kyoto 615-8540, Japan; [b]Project for Cancer Epigenomics, The Cancer Institute, Japanese Foundation for Cancer Research, Tokyo 135-8550, Japan; and [c]Department of Experimental Pathology, Institute of Medical Science, Tokyo Medical University, Tokyo 160-8402, Japan

1. B. A. Hassell *et al.*, Human organ chip models recapitulate orthotopic lung cancer growth, therapeutic responses, and tumor dormancy in vitro. *Cell Rep.* **21**, 508–516 (2017).
2. Y. Choi *et al.*, A microengineered pathophysiological model of early-stage breast cancer. *Lab Chip.* **15**, 3350–3357 (2015).
3. Y. Nashimoto *et al.*, Engineering a perfusable vascular network in a microfluidic device for a morphological analysis. *IEEJ Trans. Sens.* **138**, 275–280 (2018).
4. E. Sano *et al.*, Engineering of vascularized 3D cell constructs to model cellular interactions through a vascular network. *Biomicrofluidics* **12**, 042204 (2018).
5. D. Huh *et al.*, Reconstituting organ-level lung functions on a chip. *Science* **328**, 1662–1668 (2010).
6. Y. Xiao *et al.*, Ex vivo dynamics of human glioblastoma cells in a microvasculature-on-a-chip system correlates with tumor heterogeneity and subtypes. *Adv. Sci.* **6**, 1801531 (2019).
7. M. R. Carvalho *et al.*, Colorectal tumor-on-a-chip system: A 3D tool for precision onco-nanomedicine. *Sci. Adv.* **5**, eaaw1317 (2019).
8. Y. Nashimoto *et al.*, Vascularized cancer on a chip: The effect of perfusion on growth and drug delivery of tumor spheroid. *Biomaterials* **229**, 119547 (2020).
9. M. Astolfi *et al.*, Micro-dissected tumor tissues on chip: An ex vivo method for drug testing and personalized therapy. *Lab Chip.* **16**, 312–325 (2016).
10. D. T. T. Phan *et al.*, A vascularized and perfused organ-on-a-chip platform for large-scale drug screening applications. *Lab Chip.* **17**, 511–520 (2017).
11. C. W. McAleer *et al.*, Multi-organ system for the evaluation of efficacy and off-target toxicity of anticancer therapeutics. *Sci. Transl. Med.* **11**, eaav1386 (2019).
12. M. R. Junttila, F. J. de Sauvage, Influence of tumour micro-environment heterogeneity on therapeutic response. *Nature* **501**, 346–354 (2013).
13. Y.-H. Hsu, M. L. Moya, C. C. W. Hughes, S. C. George, A. P. Lee, A microfluidic platform for generating large-scale nearly identical human microphysiological vascularized tissue arrays. *Lab Chip.* **13**, 2990–2998 (2013).
14. H. W. Smith, W. J. Muller, Transgenic mouse models–A seminal breakthrough in oncogene research. *Cold Spring Harb. Protoc.* **12**, 1099–108 (2013).
15. A. R. Baena *et al.*, New transgenic mouse models enabling pan-hematopoietic or selective hematopoietic stem cell depletion in vivo. *Sci. Rep.* **12**, 3156 (2022).
16. J. van Blijswijk *et al.*, Altered lymph node composition in diphtheria toxin receptor-based mouse models to ablate dendritic cells. *J. Immunol.* **194**, 307–315 (2015).
17. M. Tanaka, T. Nakamura, Modeling fusion gene-associated sarcoma: Advantages for understanding sarcoma biology and pathology. *Pathol. Int.* **71**, 643–654 (2021).
18. Y. Teramura *et al.*, Identification of novel fusion genes in bone and soft tissue sarcoma and their implication in the generation of a mouse model. *Cancers* **12**, 2345 (2020).
19. Y. S. Zhang, Y.-N. Zhang, W. Zhang, Cancer-on-a-chip systems at the frontier of nanomedicine. *Drug Discov. Today* **22**, 1392–1399 (2017).
20. T. H. Kang, H. J. Kim, Farewell to animal testing: Innovations on human intestinal microphysiological systems. *Micromachines* **7**, 107 (2016).
21. A. Rongvaux *et al.*, Development and function of human innate immune cells in a humanized mouse model. *Nat. Biotechnol.* **32**, 364–72 (2014).
22. T. Fujiwara, E. Nakata, T. Kunisada, T. Ozaki, A. Kawai, Alveolar soft part sarcoma: Progress toward improvement in survival? A population-based study. *BMC Cancer* **22**, 891 (2022).
23. Z. Tan *et al.*, Clinical features and therapeutic outcomes of alveolar soft part sarcoma in children: A single-center, retrospective study. *Front. Oncol.* **12**, 1019911 (2022).
24. P.-F. Qiao, L.-H. Shen, Y. Gao, Y.-C. Mi, G.-M. Niu, Alveolar soft part sarcoma: Clinicopathological analysis and imaging results. *Oncol. Lett.* **10**, 2777–2780 (2015).
25. M. Tanaka *et al.*, ASPSCR1::TFE3 orchestrates the angiogenic program of alveolar soft part sarcoma. *Nat. Commun.* **14**, 1957 (2023).
26. A. Ogose *et al.*, Alveolar soft part sarcoma in Japan: Multi-institutional study of 57 patients from the Japanese Musculoskeletal Oncology Group. *Oncology* **65**, 7–13 (2003).
27. P.-H. Chen, X. Chen, X. He, Platelet-derived growth factors and their receptors: Structural and functional perspectives. *Biochim. Biophys. Acta.* **1834**, 2176–2186 (2013).
28. G. Maric, A. A. Rose, M. G. Annis, P. M. Siegel, Glycoprotein non-metastatic b (GPNMB): A metastatic mediator and emerging therapeutic target in cancer. *OncoTargets Ther.* **6**, 839–852 (2013).
29. G. Menasche *et al.*, Biochemical and functional characterization of Rab27a mutations occurring in Griscelli syndrome patients. *Blood* **101**, 2736–2742 (2003).
30. M. Fukuda, Rab27 effectors, pleiotropic regulators in secretory pathways. *Traffic* **14**, 949–963 (2013).
31. M. Tanaka *et al.*, Modeling alveolar soft part sarcoma unveils novel mechanisms of metastasis. *Cancer Res.* **77**, 897–907 (2017).
32. G. Bergers, S. Song, The role of pericytes in blood-vessel formation and maintenance. *Neuro Oncol.* **7**, 452–464 (2005).
33. L. S. Brown *et al.*, Pericytes and neurovascular function in the healthy and diseased brain. *Front. Cell. Neurosci.* **13**, 282 (2019).
34. G. Bergers, L. E. Benjamin, Tumorigenesis and the angiogenic switch. *Nat. Rev. Cancer* **3**, 401–410 (2003).
35. E. Ruoslahti, Specialization of tumour vasculature. *Nat. Rev. Cancer* **2**, 83–90 (2002).